IEEE Access
Multidisciplinary | Rapid Review | Open Access Journal

Received February 6, 2021, accepted February 18, 2021, date of publication February 22, 2021, date of current version March 8, 2021.

Digital Object Identifier 10.1109/ACCESS.2021.3061278

Performance of NOMA-Enabled Cognitive Satellite-Terrestrial Networks With Non-Ideal System Limitations

YERASSYL AKHMETKAZIYEV[1], GALYMZHAN NAURYZBAYEV[1], (Senior Member, IEEE), SULTANGALI ARZYKULOV[2], (Member, IEEE), AHMED M. ELTAWIL[2], (Senior Member, IEEE), KHALED M. RABIE[3], (Senior Member, IEEE), AND XINGWANG LI[4], (Senior Member, IEEE)

[1]School of Engineering and Digital Sciences, Nazarbayev University, Nur-Sultan 010000, Kazakhstan
[2]Computer, Electrical and Mathematical Science and Engineering Division, King Abdullah University of Science and Technology, Thuwal 23955, Saudi Arabia
[3]Department of Engineering, Manchester Metropolitan University, Manchester M15 6BH, U.K.
[4]School of Physics and Electronic Information Engineering, Henan Polytechnic University, Jiaozuo 454000, China

Corresponding author: Galymzhan Nauryzbayev (galymzhan.nauryzbayev@nu.edu.kz)

This work was supported in part by the Nazarbayev University Social Policy Grant and in part by the Nazarbayev University Faculty Development Competitive Research Program under Grant 240919FD3935.

ABSTRACT Satellite-terrestrial networks (STNs) have received significant attention from research and industry due to their capability of providing a stable connection to rural and distant areas, where the allocation of terrestrial infrastructures is uneconomical or difficult. Moreover, the STNs are considered as a promising enabler of fifth-generation communication networks. However, expected massive connectivity in future communication networks will face issues associated with spectrum scarcity. In this regard, the integration of cognitive radio and non-orthogonal multiple access (NOMA) techniques into STNs is considered as a promising remedy. Thereafter, in this article, we investigate NOMA-assisted cognitive STN under practical system conditions, such as transceiver hardware impairments, channel state information mismatch, imperfect successive interference cancellation, and interference noises. Generalized coverage probability formulas for NOMA users in both primary and secondary networks are derived considering the impact of interference temperature constraint and its correctness is verified through Monte Carlo simulation. Furthermore, to achieve performance fairness among the users, power allocation factors based on coverage fairness for primary and secondary NOMA users are provided. Moreover, the numerical results demonstrate superior performance compared to the ones obtained from an orthogonal multiple access scheme and examine the imperfection's impact on the system performance in terms of coverage and throughput.

INDEX TERMS Cognitive radio (CR), coverage probability, non-orthogonal multiple access (NOMA), optimization, satellite-terrestrial network (STN).

I. INTRODUCTION

Satellite-terrestrial networks (STNs) have been gaining enormous attention in recent years from both academia and industry due to their capability of providing a stable data connection over a wide coverage area, including rural and isolated areas, where the allocation of terrestrial infrastructures are profligate or challenging. Moreover, the STNs are considered as a promising enabler of future fifth-generation (5G) networks that expect a 1000-fold data traffic increase [1]. Apart from 5G technologies, the Internet-of-Things (IoT) with expected more than 40 billion devices in 2025 [2] can also benefit from the STN communications. However, in turn, this leads to a critical issue of spectrum scarcity [3]. The problem can be resolved by deploying a cognitive radio (CR) technique in the STNs, which enables spectrum sharing between the satellite and terrestrial networks [4]. Thus, the cognitive STNs (CSTNs) have been considered as a rising facilitator of future generation wireless networks.

On the other hand, to satisfy the 5G and IoT requirements, it is predictable that massive connectivity will become an essential criterion for CSTNs due to the continuously increasing number of wireless devices. Traditionally, the STN communication primarily adopts an orthogonal multiple

The associate editor coordinating the review of this manuscript and approving it for publication was Marco Martalo.

access (OMA) scheme to deliver services. However, it is considered as one of the main bottlenecks since there is a limitation in the number of servable devices due to its orthogonality. As a remedy, the non-orthogonal multiple access (NOMA) technique has been recently exploited as one of the key technologies in the future wireless networks because of its ability to serve multiple users on the same time/frequency/code resources while differentiating the users on the base of different power levels [5]–[7]. The NOMA enables non-orthogonal allocation of resources between users at the expense of additional receiver complexity, such as successive interference cancellation (SIC) mechanism, which is implemented at the user terminals in order to minimize co-channel interference (CCI) incurred by the NOMA and to successively decode the desired signals [8]. At the same time, imperfections in SIC lead to the error propagation phenomena resulting in the degraded bit error rate (BER) which is the main cost of NOMA systems [9]. In comparison with OMA schemes, in high-mobility cases, NOMA ensures robust performance gains. Particularly, OMA systems acquire no frequency-domain scheduling gain as channel state information (CSI) is obsolete, whereas NOMA provides gains as it relies on the CSI on the receiver side [10]. Furthermore, the superior performance of NOMA over conventional OMA schemes in terms of device connections and efficient utilization of spectrum has been verified by the authors in [11], [12]. NOMA is therefore recommended for use in urban environments for 5G networks with ultra-low latency and ultra-high connectivity such as IoT.

A. RELATED WORKS

During the last decade, the performance of STNs has been extensively studied in various research works. More recent articles have defined the STN as an enabler of future advanced wireless communication networks and examined its performance [13]–[17]. For example, in [13], the authors examined a relay-based STN of numerous users with multi-antennas in terms of the outage analysis and ergodic capacity, where they employ amplify-and-forward (AF) relaying with CCI considering opportunistic user scheduling with an obsolete CSI. Furthermore, the symbol error rate (SER) performance of the integrated STN with direct and cooperative modes was investigated by the authors in [4], where CCI under shadowing fading was taken into account. Moreover, in [15], closed-form analytical expressions for outage probability and throughput were obtained for an uplink STN, which employs decode-and-forward (DF) terrestrial relays. In addition, the authors in [16] and [17] investigated the security aspects of the hybrid STN by deriving analytical expressions of ergodic secrecy rate and average secrecy capacity, respectively.

1) STN AND IoT

Apart from the 5G technologies, the STN is also expected to benefit massive IoT devices. Current terrestrial networks have been evolved to provide service for a large number of devices and machines. Nevertheless, the coverage of terrestrial base stations is limited, especially, in remote environments, *e.g.*, mountains, forest, desert areas, *etc*. Thus, the integration of the STN and IoT technologies has been recently gaining special attention. For example, in [18], the authors studied the performance of the IoT and STN combination by deriving the closed-form lower bound and asymptotic outage expressions for both satellite and IoT networks. Moreover, a positive influence of the STN on the blockchain-based IoT devices was discovered by the authors in [19], where they proposed a coordinated STN to develop effective blockchains and derived a network scheduling strategy. Furthermore, the authors in [20] examined the network, where IoT sensors are linked via Low Earth Orbit (LEO) satellites and proposed control and data message overhead optimization models for the STN-assisted IoT networks.

2) CSTN

A rapidly increasing number of IoT devices lead to a crucial challenge of spectrum congestion. The deployment of the CR into STNs is currently considered as a promising remedy for this issue. Therefore, there are plenty of works where the researchers examined the CSTNs [21]–[25]. For instance, the authors in [21] explored the performance limits for the coexistence of the geostationary orbit (GEO) broadband satellite networks and terrestrial millimeter Wave (mmWave) cellular networks. In addition, they derived the outage probability and ergodic capacity for terrestrial users. Moreover, a satellite secondary network (SN) coexisting along with a terrestrial primary network (PN) was examined in [22], where the authors studied the outage performance while considering the impact of CSI uncertainty. Furthermore, the authors in [23] investigated the energy-efficient PA techniques for CSTNs by employing the quality of service (QoS) metric. The integration of relay transmission into CSTN has also been considered by several works [24], [25]. In [24], the authors considered both direct and relay communication links based on an overlay approach to numerous terrestrial users from a primary satellite source with the coexistence of a secondary transmitter-receiver pair on the ground. Additionally, underlay CSTN relay networks were analyzed in [25], where the authors analyzed the performance in terms of the two performance merits, namely, the achievable diversity order and coding gain. Further, the security issues of the CSTN considering multiple multi-antenna and uniformly distributed eavesdroppers were studied by the authors in [26] and [27].

3) STN AND NOMA

Another promising technique to resolve the problem with massive connectivity and spectrum scarcity is the NOMA, which is able to provide simultaneous service for multiple users and high efficient resource utilization. Several works have already investigated the NOMA scheme superiority in terrestrial networks [28]–[31]. For instance, the authors

in [28] investigated the downlink NOMA transmission in mmWave networks and evaluated its performance in terms of the coverage probability (CP). Furthermore, in [29], the outage performance of the CR-based NOMA was evaluated by considering the AF relaying scheme while a similar system model was examined considering the DF scheme in [30]. Inspired by this success, many researchers have recently introduced the NOMA in STNs [32]–[36]. For example, the authors in [32] evaluated the performance of such networks in terms of the outage metric by assuming that a satellite establishes simultaneous communication with numerous multi-antenna users by applying the NOMA scheme. In the same manner, the authors in [33] studied the multiple-user NOMA scheme in the STN taking into account CSI imperfections at receivers and assuming both DF and AF relaying protocols. Furthermore, a joint optimization design for a NOMA-based STN was proposed by the authors in [34], where the mmWave spectrum is shared by a satellite multicast communication network with a cellular network using the NOMA technique. Moreover, in [35], the authors considered the NOMA-assisted STN, which employs a small-cell transmission scheme under macro-cell user interference constraints, and revealed that the NOMA scheme is capable of improving the spectrum efficiency. In addition, to further maximize the spectrum utilization efficiency in the STN, the authors in [36] integrated the bandwidth compression (BC) design with NOMA, named BC-NOMA, which leads to the non-orthogonality in both power and frequency domains.

4) CSTN AND NOMA

Nonetheless, until now, very few works have evaluated the performance of NOMA-based CSTNs [37]–[40]. For instance, the authors in [37] obtained the closed-form and asymptotic outage probability expressions for both PN and SN users under the DF relay protocol, while a similar system model was evaluated in terms of the ergodic capacity considering the AF protocol in [38]. As a result, both works revealed the superior performance of the NOMA scheme over conventional OMA networks. In [39], the authors examined the overlay multi-user NOMA-assisted CSTN and investigated its superiority over traditional benchmark schemes, such as time division multiple access (TDMA) and direct satellite schemes. Additionally, they examined the influence of power allocation (PA) factors on the system performance in order to superimpose the primary receiver signals. They suggested a guideline to determine the effective value of the spectrum sharing parameter based on this analysis. Furthermore, in [40], the authors derived analytical expression using Meijer-G functions for the ergodic capacity of the NOMA-assisted CSTNs and confirmed its advantages over traditional TDMA schemes. Additionally, they examined the network performance by varying different system parameters, namely, terrestrial and satellite link configurations and PA coefficients.

5) RESIDUAL TRANSCEIVER HARDWARE IMPAIRMENTS (RTHI)

All the aforementioned works were conducted assuming perfect hardware structure at the transmission and reception nodes. In fact, the hardware struggles from many forms of impairments, such as non-linearity of in-phase/quadrature-phase imbalance (IQI), high power amplifier (HPA) and phase noises [41]–[45]. As it is stated in [44], non-ideal transceivers with imperfections induced remarkable distortions in received and transmitted signals. The RTHIs have been studied considering various system models in STNs [15], [46]–[48]. For example, the authors in [15] examined the uplink STN consisting of multiple terrestrial users which communicate with a satellite through several terrestrial DF-based relays by employing a single-antenna user and taking into account hardware imperfections at all nodes. In the same manner, the authors in [46] investigated the influence of hardware impairment (HI) on the hybrid satellite-terrestrial relay systems by conducting the performance evaluation in terms of the outage, where a GEO satellite communicates with the terrestrial destination via DF relays. Furthermore, in the context of CSTNs, the authors in [47] considered the overlay CSTN taking into account HIs at user devices, where the destructive effect on the system performance was demonstrated and the adaptive relaying protocol was proposed in order to mitigate this effect. Moreover, the influence of HIs on the performance of NOMA-based STNs was investigated in [48], where, in addition, the superiority of the NOMA over traditional schemes was demonstrated. To the best of the author's knowledge, however, there is no study yet on the impact of HIs in the joint NOMA-based CSTNs.

B. MOTIVATION AND MAIN CONTRIBUTIONS

In contrast to [37]–[40], this article examines the NOMA-based CSTN considering the aggregate transceiver distortions as well as interference temperature constraint (ITC). Moreover, to make our system model under consideration close to the realistic case, we investigate the impact of imperfect SIC, signal-to-noise ratio (SNR)-dependent and SNR-independent CSI on the performance of the NOMA-based CSTN. Hence, we summarize the key contributions of this article as follows:

- The generalized closed-form analytical expressions for the CP of the proposed NOMA-assisted CSTN are derived for both primary and secondary network users, and their correctness is verified by Monte Carlo simulation.
- Commonly, most of the recent research works on NOMA-based CSTNs assume a fixed PA scenario, where PA factors are predefined as fixed values. However, this approach is not practical in real-life cases and does not ensure fairness among all NOMA users. Therefore, we derive a closed-form solution considering non-ideal system configurations for fairness-based PA factors to provide the NOMA-enabled users with

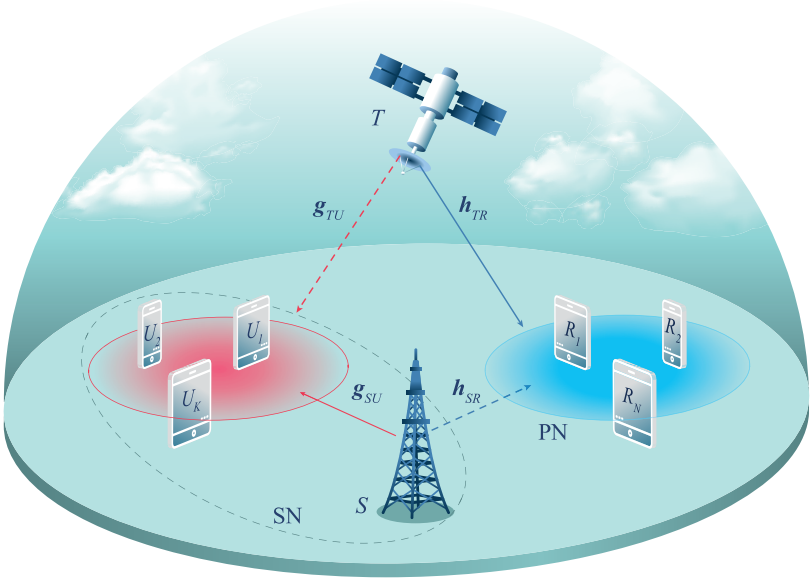

FIGURE 1. An illustration of the NOMA-assisted Cognitive STN model.

equal coverage probability. Furthermore, an algorithm to obtain fair PA factors is provided. Both methods are in good agreement with each other, which proves the correctness of a PA scheme based on the NOMA users' performance fairness.

- The influence of several system parameters on the network performance is examined using derived analytical results. And, by comparing with a benchmark OMA scheme, the advantage of NOMA is verified. Moreover, the impact of all the imperfections is examined explicitly in terms of the CP and throughput.

C. NOTATIONS AND PAPER ORGANIZATION

Notation: In this article, $f_\chi(\cdot)$ and $F_\chi(\cdot)$ represents the probability density function (PDF) and the cumulative distribution function (CDF) of a random variable (RV) χ, respectively. $\mathbb{P}_{cov}[\cdot]$ denotes the coverage probability. Also, $\Gamma(a) = \int_0^\infty t^{a-1}e^{-t}\mathrm{d}t$ [49, (8.310)], $\gamma_{inc}(a,x) = \int_0^x t^{a-1}e^{-t}\mathrm{d}t$ [49, (8.350.1)] and $\Gamma(a,x) = \int_x^\infty t^{a-1}e^{-t}\mathrm{d}t$ [49, (8.350.2)] indicate the Gamma function, the lower and upper incomplete Gamma functions, accordingly. $G_{p,q}^{m,n}(\cdot|\cdot)$ represents Meijer-G functions with a single variable.

The rest of the work is organized as follows. The system and channel modeling of NOMA-assisted CSTNs is defined in Section II while Section III derives novel closed-form analytical expressions for the coverage metric in the considered satellite and terrestrial networks. Further, Section IV presents a closed-form solution and optimization algorithm for the optimized PA factors. Section V demonstrates the numerical and simulation results to verify the correctness of the derived findings and investigate the influence of imperfections on the system performance. Finally, concluding comments and main findings of the article are drawn in Section VI.

II. SYSTEM MODEL

Consider a downlink underlay multi-user CSTN model consisting of primary and secondary networks as illustrated in Fig. 1. The satellite PN comprises the primary satellite transmitter (T) which intends to directly communicate to multiple primary users (PUs), indicated by R_n, $n \in \{1, 2, \ldots, N\}$. At the same time, the terrestrial SN consists of a secondary transmitter (S), which can access the licensed band spectrum of PUs and communicate to several secondary users (SUs), denoted by U_k, $k \in \{1, 2, \ldots, K\}$. In this case, the PUs can suffer from the aggregate interference from S while T interferes with the SUs.

A. CHANNEL MODELS

We assume that the channel estimates are obtained using linear minimum mean square error channel estimator as [50],

$$\chi = \tilde{\chi} + \epsilon, \tag{1}$$

where χ denotes the observed mismatched channel, while $\tilde{\chi}$ is a real channel estimate and ϵ indicates its estimation error, with $\mathcal{CN}(0, \lambda)$, where λ can be described considering the nominal transmit SNR ω, as $\lambda = \Phi\omega^{-\eta}$, which represents different acquisition scenarios for any constant values of $\Phi > 0$ and $\eta \geq 0$. The perfect CSI can be obtained if $\eta \to \infty$ for $\omega > 0$. Moreover, additive white Gaussian noise (AWGN), with mean zero and variance σ^2, exposes all the receivers.

1) SATELLITE DIRECT AND INTERFERENCE CHANNELS

The channels corresponding to the satellite links given by $\mathbf{g}_{TU} = [g_{T1}, g_{T2}, \ldots, g_{TK}]$ and $\mathbf{h}_{TR} = [h_{T1}, h_{T2}, \ldots, h_{TN}]$ follow the shadowed-Rician fading. Thus, the corresponding PDF is given by [51]

$$f_{|\chi_n|^2}(x) = \sum_{\ell=0}^{m_n-1} \Upsilon x^\ell e^{-\partial_n x}, \; x \geq 0, \tag{2}$$

with $\Upsilon = \frac{1}{2\bar{b}_n}\left(\frac{2\bar{b}_n m_n}{2\bar{b}_n m_n+\Omega_n}\right)^{m_n}\sum_{\ell=0}^{m_n-1}\frac{(1-m_n)_\ell(-\delta_n)^\ell}{(\ell!)^2}$ and $\partial_n = \varrho_n - \delta_n$, where $\delta_n = \frac{\Omega_n}{2\bar{b}_n(2\bar{b}_n m_n+\Omega_n)}$, $\varrho_n = \frac{1}{2\bar{b}_n}$. Here, $2\bar{b}_n$ is the average power of a multi-path component, Ω_n denotes the average power of a line-of-sight (LoS) component, and m_n represents the fading severity parameter.

We denote the antenna gain at T as G_T, with φ representing the angle between the i-th user's location and the beam center with respect to the satellite. Hence, the beam gain $G_i(\varphi)$ is expressed as [52]

$$G_i(\varphi) = G_{i,\max}\left(\frac{J_1(u)}{2u} + 36\frac{J_3(u)}{u^3}\right)^2, \tag{3}$$

where $u = 2.07\frac{\sin\varphi}{\sin\varphi_{3\text{dB}}}$, $\varphi_{3\text{dB}}$ is the 3-dB angle for the beam, and $J_l(\cdot)$ is the first-kind Bessel function of order l.

2) TERRESTRIAL DIRECT AND INTERFERENCE CHANNELS

The terrestrial links given by $\mathbf{g}_{SU} = [g_{S1}, g_{S2}, \ldots, g_{SK}]$ and $\mathbf{h}_{SR} = [h_{S1}, h_{S2}, \ldots, h_{SN}]$ are presumed to abide the Nakagami-m fading. Hence, the channel gains (*i.e.*, squared values) are Gamma RVs with the PDF given by

$$f_{|\chi_k|^2}(y) = \frac{y^{m_k-1}e^{-\frac{y}{\nu}}}{\Gamma(m_k)\nu^{m_k}}, \tag{4}$$

where m_k and ν stand for the shape and scale parameters, respectively.

In addition, the sectorized antenna pattern has been used to model analog beamforming between communicating nodes as $G(\theta) = G_m$, when $\theta \le \theta_b$; otherwise, $G(\theta) = G_s$, where G_m and G_s denote the main and side lobe gains,[1] respectively. θ is the angle of a boresight direction, while θ_b indicates the antenna beamwidth. For convenience, we assume that the terrestrial station interferes with the PUs with side lobe gain, while main lobe gain is exploited in the terrestrial direct links.

B. SIGNAL AND SINDR MODELS

1) SATELLITE PRIMARY NETWORK

The satellite T and N terrestrial end-users ($R_{n,\ n\in\{1,\ldots,N\}}$) comprise the downlink satellite PN that employs the NOMA concept by broadcasting a superposed signal $x = \sum_{n=1}^{N}\sqrt{\alpha_n}x_n$, where x_n and α_n denote the message devoted for the n-th user and the corresponding PA coefficient (with $\alpha_1 > \alpha_2 > \ldots > \alpha_N$ s.t. $\sum_{n=1}^{N}\alpha_n = 1$).

Hence, considering the CSI imperfections in (1), the received signal at R_i, for $i \in \{1, \ldots, N\}$, can be written as

$$y_i = \left(\tilde{h}_i + \epsilon_i\right)\sqrt{P_T G_T G_i(\varphi) L}\left(\sum_{n=1}^{N}\sqrt{\alpha_n}x_n + \mu_i\right) + h_{Si}\sqrt{P_S G_S \bar{G}_i d_{Si}^{-\tau}}\,(s_k + \bar{\mu}_i) + n_i, \tag{5}$$

where $n_i \sim \mathcal{CN}\left(0, \sigma_i^2\right)$ denotes the AWGN term. $\mu_i \sim \mathcal{CN}\left(0, \kappa_i^2\right)$ and $\bar{\mu}_i \sim \mathcal{CN}\left(0, \bar{\kappa}_i^2\right)$ represent the impact of residual HIs by the aggregate distortion noises, where κ_i and $\bar{\kappa}_i$ denote the HI rates detected in the corresponding transmitter-receiver pairs' communication links. Moreover, L denotes path-loss which follows the Friis' law for free-space propagation states [52].

Then, considering non-ideal SIC, the instantaneous signal-to-interference-noise-distortion ratio (SINDR) at R_i to decode message x_n, for $n \leqslant i$, is expressed by arranging $\rho_i = P_T G_T G_i(\varphi) L$, $\bar{\rho}_i = P_S G_S G_i d_{SRi}^{-\tau}$, $X_i = |\tilde{h}_{TR_i}|^2$, $Y_i = |h_{SR_i}|^2$, $a = \alpha_n\rho_i$, as follows

$$\gamma_{i\to n} = \frac{aX_i}{bX_i + \Sigma_i + cY_i}, \tag{6}$$

where $\Sigma_i = \rho_i\left(1+\kappa_i^2\right)\sigma_\epsilon^2 + \sigma_i^2$ stands for the power levels of the channel error (*i.e.*, σ_ϵ^2) and the AWGN noise (*i.e.*, σ_i^2), respectively. The interference power factor received from S is given by $c = \left(1+\bar{\kappa}_{SR_i}^2\right)\bar{\rho}_i$, while $b = \rho_i\mathcal{A}$ represents the SIC-based interference level, with $\mathcal{A} = \left(\Psi_n + \tilde{\Psi}_n + \kappa_i^2\right)$, where $\Psi_n = \sum_{t=n+1}^{N}\alpha_t$, and $\tilde{\Psi}_n = \sum_{l=1}^{n-1}\xi_l\alpha_l$, with $0 \le \xi \le 1$ [31]. Note that R_1 decodes its own message by considering the messages' of the other users as a noise and defining $\Psi_1 = \sum_{t=2}^{N}\alpha_t$ and $\tilde{\Psi}_1 = 0$. On the other hand, only R_N needs to decode message x_N, subject to $\Psi_N = 0$ and perfect/imperfect SIC realizations given by $\tilde{\Psi}_n = \sum_{l=1}^{n-1}\xi_l\alpha_l$.

2) TERRESTRIAL SECONDARY NETWORK

On the other hand, the terrestrial SN consists of the secondary transmitter S and K NOMA end-users ($U_{k,\ k\in\{1,\ldots,K\}}$), when the superimposed signal $s = \sum_{k=1}^{K}\sqrt{\beta_k}s_k$ is sent to all intended SUs, where s_k and β_k indicate the message dedicated for the k-th SU and the corresponding PA coefficient (with $\beta_1 > \beta_2 > \ldots > \beta_K$ s.t. $\sum_{k=1}^{K}\beta_k = 1$). G_S is the antenna gain at S. In the same manner, the received signal at U_j, for $j \in \{1, \ldots, K\}$, can be written as

$$r_j = \left(\tilde{g}_j + \epsilon\right)\sqrt{P_S G_S G_{D_j} d_j^{-\tau}}\left(\sum_{k=1}^{K}\sqrt{\beta_k}s_k + \bar{\mu}_i\right) + g_{PD}\sqrt{P_T G_T G_D(\varphi) L}\left(x_n + \mu_j\right) + n_j. \tag{7}$$

Hence, we can express the SINDR at U_j, for $j \in \{1, \ldots, K\}$, to detect message s_k from S as follows

$$\psi_{j\to k} = \frac{W_1 Z_j P_S}{P_S\left(W_2 Z_j + E\right) + CQ_j + \sigma_j^2}, \tag{8}$$

where $Z_j = |\tilde{g}_j|^2$, $Q_j = |g_{T_j}|^2$, and $W_1 = \beta_k G_S G_{D_j} d_j^{-\tau}$. The power of channel error is denoted by $E = G_S G_{D_j} d_j^{-\tau}\left(1+\bar{\kappa}_i^2\right)\sigma_\epsilon^2$ and σ_j^2 is AWGN noise power. $W_2 = G_S G_{D_j} d_j^{-\tau}\bar{\mathcal{A}}$ stands for the SIC-based interference, with $\bar{\mathcal{A}} = \left(\Psi_j + \tilde{\Psi}_j + \bar{\kappa}_i^2\right)$, whereas $C = \left(1+\kappa_{T_j}^2\right)P_T G_T G_D(\varphi) L$ denotes the interference term received from T.

[1] It is assumed that an antenna gain has a constant value in the frame of given main or side lobe sectors.

III. COVERAGE PROBABILITY

A. SATELLITE PRIMARY NETWORK

By definition, the coverage is defined as the probability that the SINDR value greater than a predefined SNR-associated rate threshold, which can be expressed as $v = 2^{\mathcal{R}} - 1$, where $\mathcal{R}$ denotes the data rate threshold [54]. Thus, by applying (6), the CP of decoding message x_n by R_i can be determined as

$$\mathbb{P}_{cov,i}(v) = Pr\left[\gamma_{i\to n} > v\right], 0 < n \leq i. \tag{9}$$

Proposition 1: Considering imperfect SIC/CSI/HI, we can express the closed-form CP expression for the primary user of interest as in (10), as shown at the bottom of the page.

Proof: Derivation details are drawn in Appendix A. ■

B. TERRESTRIAL SECONDARY NETWORK

The CP for U_K can be expressed using (8) and considering ITC as in (11), as shown at the bottom of the page, where $S_i = \frac{I_{ITC}^{[i]}}{Y_i}$ and $P_S = \min\left(\bar{P}_S, S^*\right)$ by assuming $S^* = \max(S_1, S_2, \ldots, S_N)$. Further, we denote $I_{ITC}^{[i]} = I_{ITC} d_{SR_i}^{\tau}$ and $Y_i = |h_{SR_i}|^2$.

For the convenience, we simplify the expression using the following definitions: $T_1 = \frac{v(EP_s+\sigma_j^2)}{P_s(W_1-vW_2)}$, $T_2 = \frac{vC}{P_s(W_1-vW_2)}$, $J_1 = \frac{v\sigma_j^2}{I_{ITC}^{[i]}(W_1-vW_2)}$, $J_2 = \frac{vC}{I_{ITC}^{[i]}(W_1-vW_2)}$, $J_3 = \frac{vI_{ITC}^{[i]}E}{I_{ITC}^{[i]}(W_1-vW_2)}$, and $\Lambda = \frac{I_{ITC}^{[i]}}{\bar{P}_s}$.

Proposition 2: The CP in the SN given by (11) can be expressed in closed-form considering ITC as sum of (12) and (13), as shown at the bottom of the page, where, for the sake of brevity, the terms A and B are demonstrated separately.

$$A = 1 - \left(\sum_{\ell=0}^{m_n-1} \Upsilon \ell! \partial_n^{-\ell-1} - \sum_{\ell=0}^{m_n-1} \sum_{p=0}^{m_0-1} \sum_{n=0}^{p} M_A T_2^n \Upsilon (n+\ell)! \times \left(\frac{T_2}{\nu_0} + \partial_n\right)^{-n-\ell-1} \right) \frac{\gamma\left(m_k, \frac{\Lambda}{\nu}\right)}{\Gamma(m_k)}. \tag{12}$$

Proof: A full derivation can be found in Appendix B. ■

IV. ADAPTIVE POWER ALLOCATION

A. CLOSED-FORM APPROACH

Many previous works on NOMA-based CSTNs assumed the fixed PA schemes, where the power is allocated to the users with respect to their channel conditions; therefore, involved users obtain different performance rates, as expected. Contrarily, for fairness purposes, it is important to ensure that all served users experience the same performance. Thus, in this article, we derive a closed-form fairness-based PA solution to provide equal coverage probability to NOMA users. In order to implement that, we use the SINDR of NOMA users by making them equal to some auxiliary SINDR, $\ddot{\gamma}$. It is worthwhile mentioning that, in general, it is recommended to apply NOMA for the two-user case only due to the non-linear processing complexity dependent on the number of involved end-users [55]. This complexity of the system becomes more critical when errors exist during the SIC process [56]. At the same time, for the considered system model with imperfect SIC, the derivation of the closed-form fairness-based PA factors becomes intractable for the cases with more than 2 users. Hence, considering the abovementioned discussion, we provide a closed-form fairness-based PA factor solution for a two-user case with their SINDRs, γ_1 and γ_2, which can be defined using (6) as

$$\gamma_1 = \frac{aX_1}{bX_1 + \Sigma_1 + cY_1}, \tag{14}$$

$$\gamma_2 = \frac{aX_2}{bX_2 + \Sigma_2 + cY_2}. \tag{15}$$

Thus, the following problem can be formulated to find the auxiliary fair PA factors and SINDR:

$$\min \ |\gamma_1 - \gamma_2| \tag{16}$$

$$\text{s.t. } \gamma_i = \ddot{\gamma}, \quad i \in \{1, 2\}, \tag{16a}$$

$$\sum_i \alpha_i \leq 1. \tag{16b}$$

$$\mathbb{P}_{cov,i}^{\text{PN}}(v) = 1 - \sum_{\ell=0}^{m_n-1} \frac{\Upsilon \ell!}{\partial_n^{\ell+1}} + \sum_{\ell=0}^{m_n-1} \sum_{p=0}^{\ell} \frac{\ell!}{p!} \frac{\Upsilon e^{-I(i)\Sigma_i(\partial_n)}}{\partial_n^{\ell-p+1}} \sum_{t=0}^{p} \frac{(I(i))^p p! \left(\Sigma_i\right)^{p-t} c^t}{t!(p-t)!} \frac{\Gamma(t+m_k)}{\Gamma(m_k) v^{m_k}} \left(\frac{1}{\nu} + I(i)\partial_n c\right)^{-t-m_k} \tag{10}$$

$$\begin{aligned} \mathbb{P}_{cov,j}^{\text{SN}}(v) &= Pr\left(\frac{W_1 Z_j P_S}{P_S\left(W_2 Z_j + E\right) + CQ_j + \sigma_j^2} > v, \bar{P}_s < S_i\right) + Pr\left(\frac{W_1 Z_j S_i}{S_i\left(W_2 Z_j + E\right) + CQ_j + \sigma_j^2} > v, \bar{P}_s > S_i\right) - 1 \\ &= \underbrace{Pr\left(Z_j > (T_1 + T_2 Q_j), Y_i < \Lambda\right)}_{A} + \underbrace{Pr\left(Z_j > (J_1 Y_i + J_2 Q_j Y_i + J_3), Y_i > \Lambda\right) - 1}_{B}. \end{aligned} \tag{11}$$

$$B = -\frac{\Gamma(m, \frac{\Lambda}{\nu})}{\Gamma(m)} \sum_{\ell=0}^{m_n-1} \Upsilon \ell! \partial_n^{-\ell-1} + \sum_{p=0}^{m_0-1} \sum_{t=0}^{p} M_B \sum_{i=0}^{t} \binom{t}{i} J_1^{t-i} J_2^i \frac{\Gamma(t+m)}{\Gamma(m) v^m} e^{-\left(\frac{1}{\nu} + \frac{J_1}{\nu_0}\right)\Lambda} \sum_{\ell=0}^{m_n-1} \sum_{j=0}^{t+m-1} \frac{\Lambda^j \Upsilon}{j!} \times \frac{V_2 \Omega^{-(i+\ell+1)}}{\Gamma(-j+t+m)} G_{1,2}^{2,1}\left(\frac{\frac{J_2\Lambda}{\nu_0} + \partial_n}{\Omega} \middle| \begin{matrix} 1-(i+\ell+1) \\ 0, -(i+\ell+1) + (-j+t+m) \end{matrix}\right) \tag{13}$$

TABLE 1. The Fairness-Based Closed-Form PA Factors

no. users	α_n
2	$\alpha_1 = \ddot{\gamma}\bar{I}_1 + \ddot{\gamma}^2\bar{I}_2$ $\alpha_2 = \ddot{\gamma}\bar{I}_2$
3	$\alpha_1 = \ddot{\gamma}\bar{I}_1 + \ddot{\gamma}^2\bar{I}_2 + \ddot{\gamma}^2\bar{I}_3(1+\ddot{\gamma})$ $\alpha_2 = \ddot{\gamma}\bar{I}_2 + \ddot{\gamma}^2\bar{I}_3$ $\alpha_3 = \ddot{\gamma}\bar{I}_3$
4	$\alpha_1 = \ddot{\gamma}\bar{I}_1 + \ddot{\gamma}^2\bar{I}_2 + \ddot{\gamma}^2\bar{I}_3(1+\ddot{\gamma}) + \ddot{\gamma}^2\bar{I}_4(1+\ddot{\gamma})^2$ $\alpha_2 = \ddot{\gamma}\bar{I}_2 + \ddot{\gamma}^2\bar{I}_3 + \ddot{\gamma}^2\bar{I}_4(1+\ddot{\gamma})$ $\alpha_3 = \ddot{\gamma}\bar{I}_3 + \ddot{\gamma}^2\bar{I}_4$ $\alpha_4 = \ddot{\gamma}\bar{I}_4$

The solution steps for (16) are given as follows. First, we make $\gamma_1 = \gamma_2 = \ddot{\gamma}$ that results in

$$\frac{aX_1}{bX_1 + \Sigma_1 + cY_1} = \ddot{\gamma}, \text{ and} \tag{17}$$

$$\frac{aX_2}{bX_2 + \Sigma_2 + cY_2} = \ddot{\gamma}. \tag{18}$$

Next, using (17) and (18), we derive α_1 and α_2 as

$$\alpha_1 = \ddot{\gamma}\alpha_2 + \ddot{\gamma}\bar{I}_1, \tag{19}$$

$$\alpha_2 = \ddot{\gamma}\xi_1\alpha_1 + \ddot{\gamma}\bar{I}_2, \tag{20}$$

where $\bar{I}_i = \frac{\Xi}{|\tilde{h}_i|^2}$ and $\Xi = \kappa_i^2|\tilde{h}_i|^2 + \frac{\Sigma_i + cY_i}{\rho_i}$, with $i \in \{1, 2\}$. Then, after substituting (20) into (19), α_1 can be rewritten as

$$\alpha_1 = \frac{\ddot{\gamma}^2\bar{I}_2 + \ddot{\gamma}\bar{I}_1}{1 - \ddot{\gamma}^2\xi_1}. \tag{21}$$

Now, substituting (21) into (20), we obtain α_2 as

$$\alpha_2 = \frac{\ddot{\gamma}^3\xi_1\bar{I}_2 + \ddot{\gamma}^2\xi_1\bar{I}_1}{1 - \ddot{\gamma}^2\xi_1} + \ddot{\gamma}\bar{I}_2. \tag{22}$$

Finally, the optimal SINDR can be expressed by inserting (21) and (22) into $\alpha_1 + \alpha_2 \leq 1$ as

$$\ddot{\gamma} = \frac{\sqrt{(\bar{I}_1 + \bar{I}_2)^2 - (\bar{I}_1 + \bar{I}_2) - 4(\bar{I}_2 + \bar{I}_1\xi_1 + \xi_1)}}{2(\bar{I}_2 + \bar{I}_1\xi_1 + \xi_1)}. \tag{23}$$

One can obtain optimal α_1 and α_2 by inserting (23) into (21) and (22), respectively. Note that we derive the PA factors for two-user case taking into account the imperfect SIC; however, for more users, this problem is intractable. At the same time, it is pertinent to mention that, when ideal SIC is of interest, the PA factors for two-, three- and four-user cases are drawn in Table 1, accordingly.

In the same manner, optimal β_k for terrestrial secondary users can be derived using their SINDRs, ψ_k, defined in (8).

TABLE 2. Simulation Parameters

Parameter	Value
Terrestrial channel parameter, m_0	4
Satellite channel parameters, $\{m_i, b_i, \Omega_i\}$	$\{5, 0.251, 0.279\}$
Terrestrial antenna gains, $\{G_m, G_s\}$	$\{12, -1.1092\}$ dB
Satellite antenna gains, $\{G_T, G_{i,max}\}$	$\{4.8, 54\}$ dB
Threshold, $\{\zeta_{NOMA}, \zeta_{OMA}\}$	$\{3, 12\}$ dB
PA factors, $\{\alpha_1/\beta_1, \alpha_2/\beta_2\}$	$\{0.7, 0.3\}$
Path-loss exponent, τ	2
Orbit height, D	35786 km
ST-to-R_N distance, $\{d_{R_1}, d_{R_2}\}$	$\{250, 200\}$ m
ST-to-U_K distance, $\{d_{U_1}, d_{U_2}\}$	$\{200, 150\}$ m
3-dB angle, φ_{3dB}	0.4°
Carrier frequency, f_c	2 GHz
Interference noise power	10 dB
Temperature, $\mathcal{T}$	300 K
Carrier bandwidth, $\mathcal{W}$	15 MHz

B. CVX APPROACH

Here, we investigate the fairness-based PA factors which provide a fair CP for both types of users by compiling with the ITC constraint using geometric programming. The PA problems for the PN and SN can be formulated as

$$\begin{aligned} \mathbf{P_1}: \max_{\alpha_n, \ddot{\gamma}} \ & \ddot{\gamma} \\ \text{s.t. } P_1^1: \ & \gamma_n \geq \ddot{\gamma}, \quad \forall n \in \{1, \ldots, N\} \\ P_1^2: \ & \sum \alpha_n \leq 1 \\ P_1^3: \ & \alpha_n \in [0, 1], \quad \forall n, \end{aligned} \tag{24}$$

and

$$\begin{aligned} \mathbf{P_2}: \max_{\beta_k, \ddot{\psi}} \ & \ddot{\psi} \\ \text{s.t. } P_2^1: \ & \psi_k \geq \ddot{\psi}, \quad \forall k \in \{1, \ldots, K\} \\ P_2^2: \ & \sum \beta_k \leq 1 \\ P_2^3: \ & \beta_k \in [0, 1], \quad \forall k \end{aligned} \tag{25}$$

where we handle the max-min objective by setting the objectives to auxiliary variables $\ddot{\gamma}$ and $\ddot{\psi}$ and enforcing all SINDRs to be not less than $\ddot{\gamma}$ in P_1^1 and $\ddot{\psi}$ in P_2^1 for the PN and SN, respectively. P_1^2 and P_2^2 represent the maximum transmission power levels available at the source nodes. P_1^3 and P_2^3 show that the PA factors α_n and β_k obtain values ranging from 0 to 1. We solve $\mathbf{P_1}$ and $\mathbf{P_2}$ numerically by altering P_1^1 and P_1^2 into $1/\gamma_n \leq 1/\ddot{\gamma}$ and $1/\psi_k \leq 1/\ddot{\psi}$, respectively, to put inequality constraints in the form of posynomials.

V. RESULTS DISCUSSION

This section provides the numerical results on the CP for the system model under consideration designated by the simulation framework drawn in Table 2, which mainly follows the parameters listed in [15], [52], unless specified otherwise. Also, it should be noted that the transmit SNR in the following plots are defined as $\frac{P_T}{\sigma_i^2}$ and $\frac{P_S}{\sigma_j^2}$ for the PN and SN,

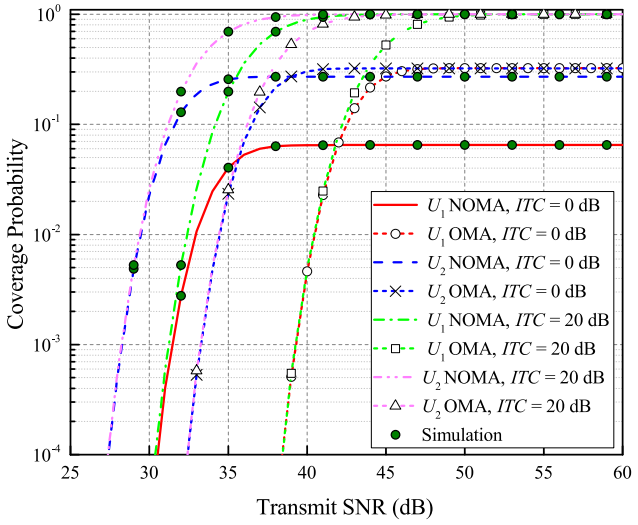

FIGURE 2. Coverage probability versus the transmit SNR for the NOMA- and OMA-based SN with *ITC* = {0, 20} dB.

respectively. Moreover, we verify our derived analytical expressions (10) and (11) through Monte Carlo simulations.

In Fig. 2, we compare the results on the coverage probability of the SUs based on the analytical findings derived in Section III with those related to the OMA scheme for the two-user case[2] under different ITC levels. It is seen from the plot that a better CP for the NOMA-based network is achieved at a higher value of the ITC. On the other hand, when a smaller ITC is imposed, the CP degrades by showing a saturation at lower SNR values. Moreover, one can observe that the NOMA-based network has superiority over the OMA in terms of the CP. However, it can be noticed that, for U_1, the coverage saturation for the NOMA-assisted network starts at the lower levels of transmit SNR in contrast to the SNR rate for the OMA network. It can be justified by the ITC equation, where the transmit power of 0.5 P_s increases the level of the ITC impact at S. In addition, it should be noted that our analytical findings perfectly coincide with the Monte Carlo simulations which verify the correctness of our derivations.

In Fig. 3, the CP comparison of the primary and secondary users with fixed and adaptive fairness-based PA factors obtained in Section IV-A is illustrated. In the case of fixed PA factors, it can be seen that the second users (in red color) in both PN and SN demonstrate superior coverage performance which can be explained by the influence of chosen simulation parameters. Commonly, many research works assume fixed PA factors, where power is allocated among the users based on their channel conditions; hence, each user achieves various levels of performance. However, it is not realistic and the most efficient scenario. Therefore, we apply the fairness-based PA factors obtained from Section IV-A in order to provide fair and equal CP to all users. Thus, from Fig. 3, one can observe that the PA scheme provides both users in the PN and SN with an equal CP and allows them to achieve the performance rate somewhere between the CP curves related to the scenario with fixed PA factors. With this in mind, we decide to apply the fairness-based PA factors to all the forthcoming results.

Fig. 4 compares the coverage performance of the optimized primary and secondary users. Particularly, the CP results for two-, three-, four-user NOMA cases are plotted by utilizing the optimized closed-form PA factors from Section IV-A. Moreover, we plot the CP results for two-, three-, four- and five-user NOMA scenarios solving $\mathbf{P_1}$ and $\mathbf{P_2}$ in Section IV-B. It should be noted that, in the N-user NOMA scenario, each coverage curve represents the identical (overlapped) curves for all and each of users, *e.g.*, if $K = 3$, then it is true for users U_1, U_2 and U_3. Furthermore, one can clearly notice that the two-user NOMA scenario greatly outperforms the NOMA cases in both PN and SN, with a higher advance in the former. It should be noted that we can further expand our results by obtaining the CP metric for more than five users by deploying geometric programming from Section IV-B. However, it is obvious that with a higher number of users, the coverage performance deteriorates significantly. Due to these findings, the consideration of multiple NOMA users may be infeasible; therefore, for further performance examination, we consider only the adaptive two-user NOMA scenario.

Fig. 5 illustrates the influence of CSI imperfections on the CP performance for the PN. Particularly, Fig. 5 demonstrates the influence of SNR-independent CSI mismatches by adjusting $\eta = 0$. It is clearly noticeable that the CP performance deteriorates with increasing Φ and its impact becomes tangible as the transmit SNR increases. It is apparent that imperfect CSI has an enormous effect on the system performance. However, this influence of Φ almost invisible at high SNR levels. In its turn, when $\eta \neq 0$, CSI becomes SNR-dependent. Moreover, Fig. 5 illustrates that the higher rate of η leads to better system performance. Contrarily, in the case of equal η values, the growth of Φ leads to the noticeable deterioration of the CP performance. However, it is apparent that η has much more effect on the performance than Φ. It is worth mentioning that all curves in the SNR-dependent case level out on the same CP at high SNR values.

Fig. 6 shows the impact of CSI mismatch on the performance of secondary users. The plot depicts the SNR-independent/dependent CSI scenarios. When $\eta = 0$, meaning that the channel error variance is independent of the transmit SNR, it is observed that Φ affects the system performance quite noticeably. However, Φ does not have a significant effect on the CP performance at high SNR values. In its turn, when $\eta \neq 0$, CSI becomes SNR-dependent again. Here, one can observe that the increase of η leads to the improvement of system performance. Furthermore, in the case of equal η values, the growth of Φ causes the CP degradation. However,

[2]For the sake of simplicity, we consider only two PUs and two SUs with fixed PA factors due to the following reason. Serving multiple NOMA nodes can be impractical in real-time communication due to the fact that, at a receiver side, the processing complexity of the SIC increases non-linearly by raising the number of users [55]. In addition, the issue becomes more crucial when the SIC error exists [31].

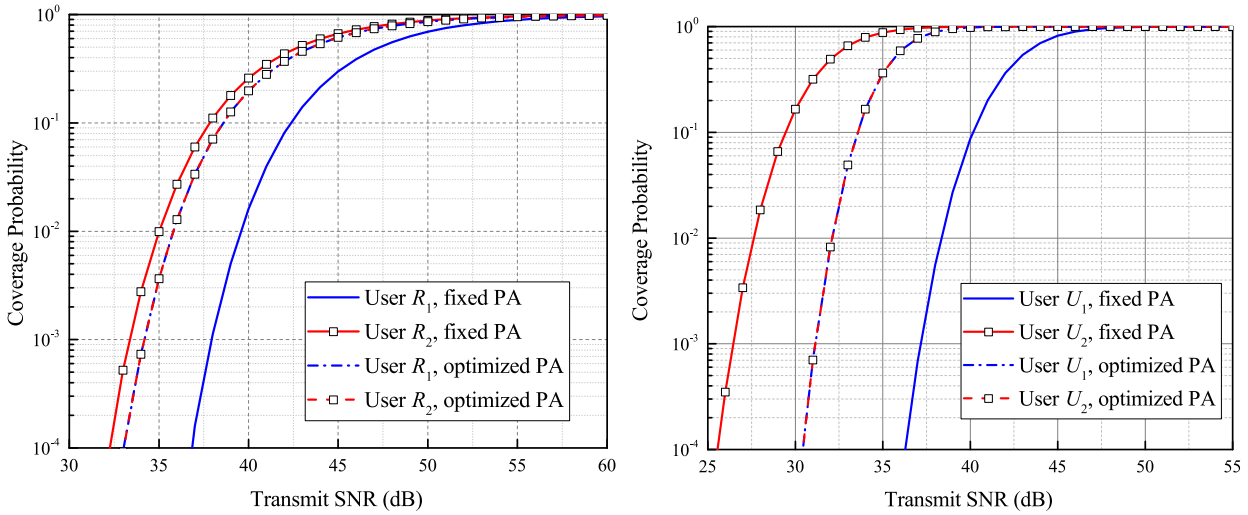

(a) Coverage of the PN users with fixed and adaptive PA factors.

(b) Coverage of the SN users with fixed and adaptive PA factors.

FIGURE 3. Coverage probability versus the transmit SNR for the PN and SN with different PA schemes.

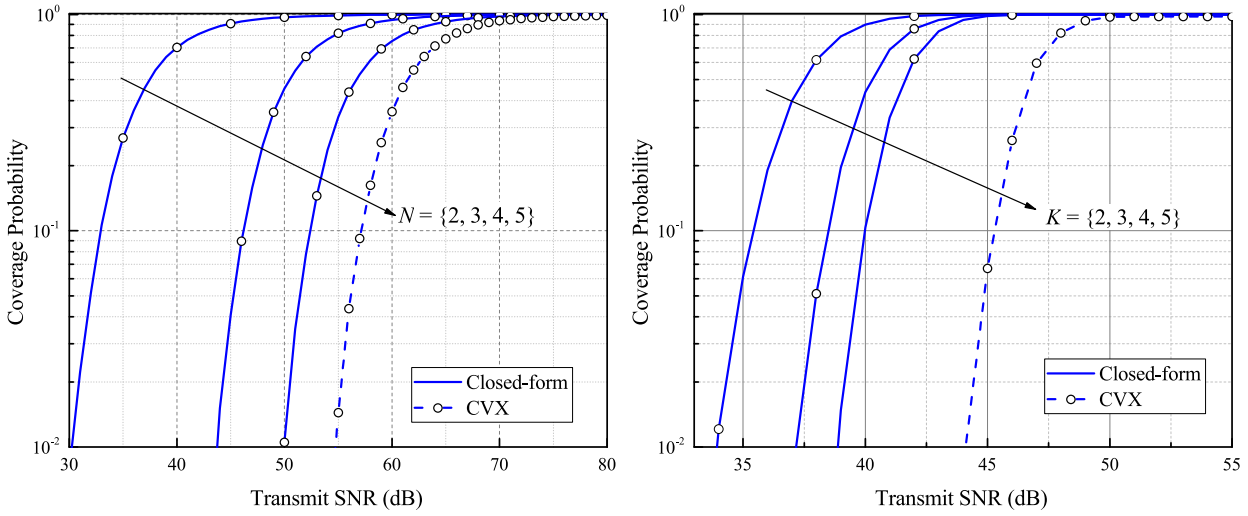

(a) Coverage for the PN with different number of users.

(b) Coverage for the SN with different number of users.

FIGURE 4. Coverage probability versus the transmit SNR for the PN and SN with different numbers of users.

it is obvious that η has much more influence on the performance than Φ. It should be noted that, after 45 dB, all the CP curves are equal to each other in both SNR-independent and -dependent cases.

In Fig. 7, we examine the influence of the different levels of HI on the CP performance in the PN and SN. Particularly, the HI level was set to three different scenarios with $\kappa = \{0, 0.15, 0.3\}$. As expected, the CP of both primary and secondary users deteriorates in the presence of HI. It should be noted that HIs have a low impact at high SNRs and all the curves of the PN and SN level out on the same CP at 60 dB and 47 dB, respectively. Moreover, one can observe that a small value of HI has a marginal impact. However, it is still noticeable that a higher rate of HI can greatly degenerate the overall system coverage performance. Thus, the most obvious shift applies to $\kappa = 0.3$, whereas the other hardware realizations can be characterized by a marginal deviation from the ideal case.

In Fig. 8, we study the impact of various Nakagami-m channel parameters and the SIC influence in the ideal case, namely, with the $\xi = \{0, 0.05, 0.1\}$, on the performance of the terrestrial SN. It is clearly observable that a higher m parameter leads to a better performance with $m = 4$ demonstrating the best CP rates. Additionally, the influence of various SIC scenarios is investigated for the ideal case. With respect to the obtained results, subject to flawed SIC, the performance of U_2 deteriorates when ξ increases, as expected. It is worth mentioning that, at the higher level of transmit SNR, imperfect SIC has a low impact on the CP.

In modern wireless networks, the development of a HI-free system is an extraordinarily expensive and challenging task. Nevertheless, there are some devices that are resistant to the

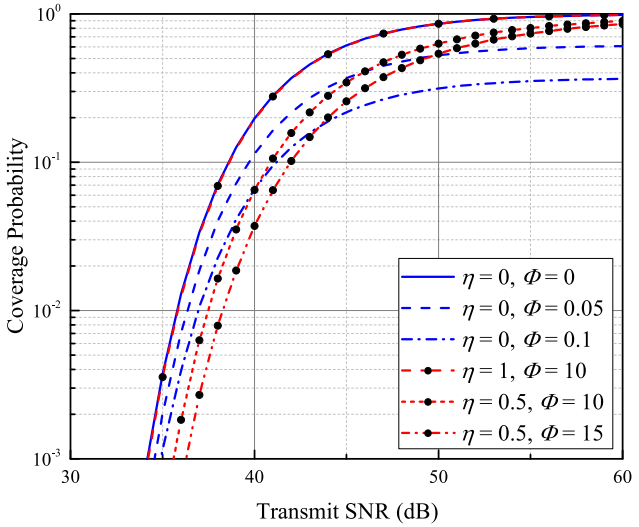

FIGURE 5. Coverage probability versus the transmit SNR for the PN over different CSI scenarios.

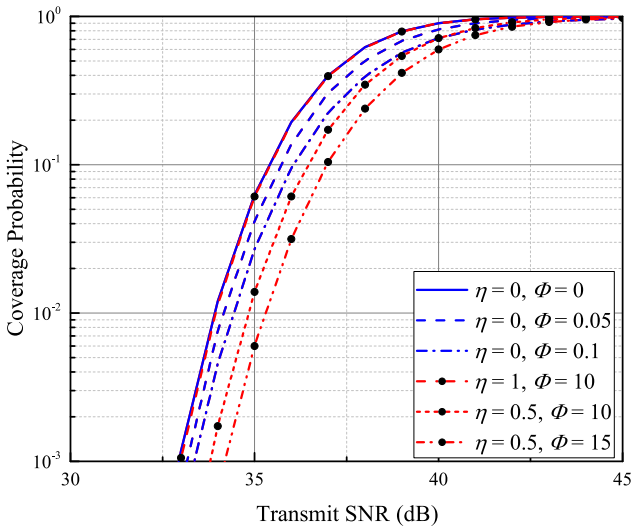

FIGURE 6. Coverage probability versus the transmit SNR for the SN under different CSI scenarios.

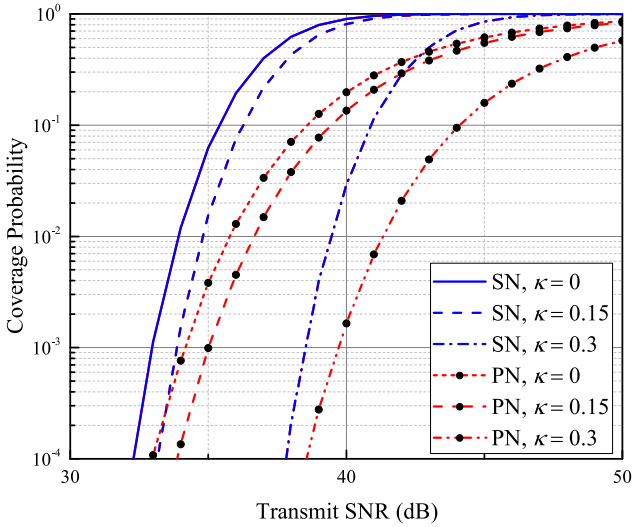

FIGURE 7. Coverage probability versus the transmit SNR for the PN and SN under different HI scenarios.

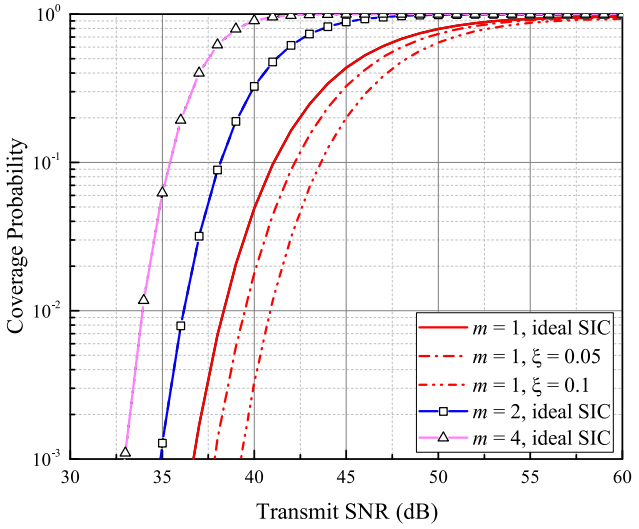

FIGURE 8. Coverage probability versus the transmit SNR for the SN under different Nakagami-*m* and SIC scenarios.

HI up to certain levels assuming that their QoS requirements are satisfied. Therefore, Fig. 9 illustrates the failure probability of the system performance versus HI under various transmit power levels for the PN and SN. Here, we assume that the failure probability threshold of the system under consideration is 10^{-2}. From both plots, it can be clearly seen that taking higher transmit power allows us to obtain lower failure probability, even though HI deteriorates the system performance and increases the possibility of failure. Thus, 65 dB for the PN and 45 dB for the SN provide the lowest failure probabilities which mainly satisfy the system's HI tolerance level in the ideal case. In addition, from Fig. 9, one can observe the impact of imperfect SIC on failure probability. As it is expected, the possibility that failure occurs increases as the value of ξ goes up. For example, $\xi = 0.1$ causes the greatest system degradation and a very high level of failure probability for both primary and secondary networks even with the high level of transmit SNR.

In Fig. 10, we plot the CP versus the predefined data rate threshold in bps/Hz at the transmit SNR of 40 dB considering various imperfect CSI scenarios for both PN and SN. It is obvious that the CP deteriorates with an increasing threshold, as expected. Furthermore, in the plots, both SNR-dependent/independent CSI cases were considered. Thus, $\eta = 0$ means that CSI is SNR-independent. In this case, the crumbling impact of Φ on the system performance can be clearly noticed. Contrarily, when $\eta \neq 0$, CSI becomes dependent on the transmit SNR. The figure demonstrates that an increase of η leads to the improvement of the system coverage. However, in the case of equal η values, one can notice the degradation of CP performance as Φ increases. It becomes obvious that Φ has a way lower influence on the

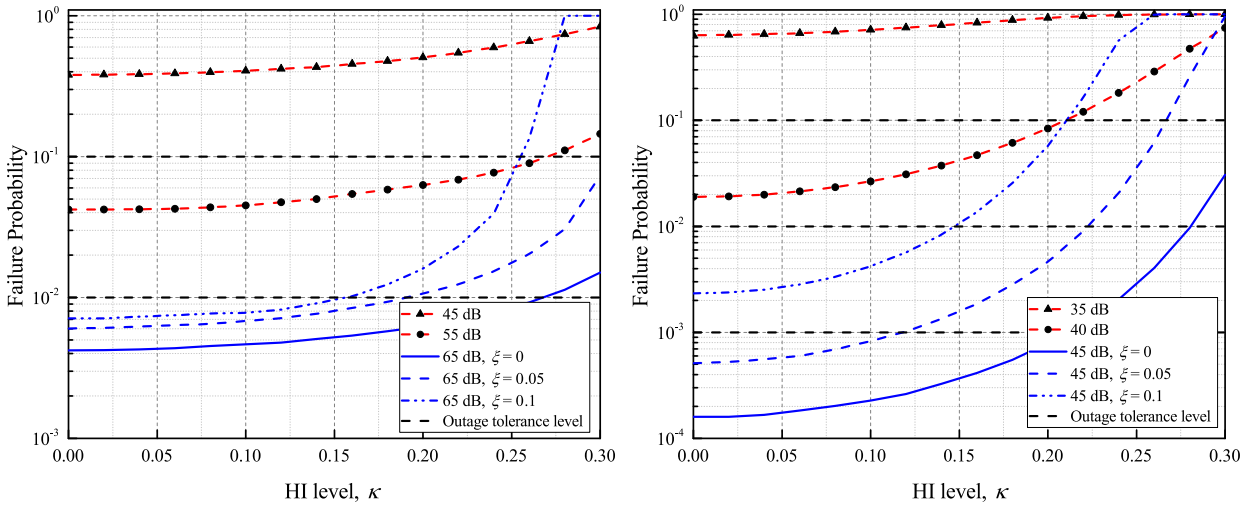

(a) Failure probability versus HI for the PN.

(b) Failure probability versus HI for the SN.

FIGURE 9. Failure probability versus HI under different transmit power levels and SIC scenarios.

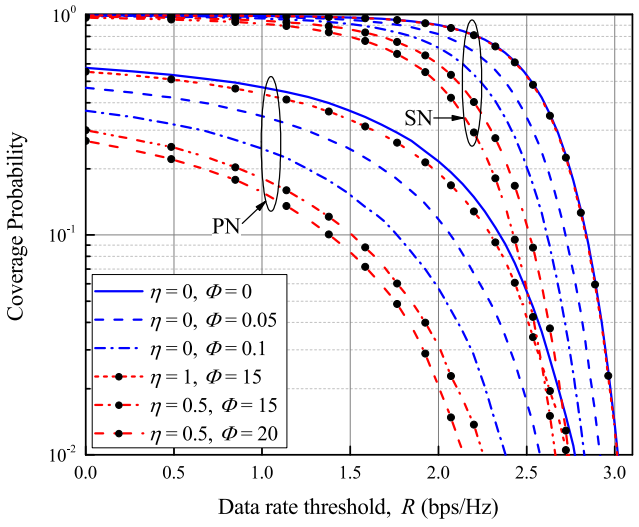

FIGURE 10. Coverage probability versus the rate threshold for the PN and SN under different CSI scenarios.

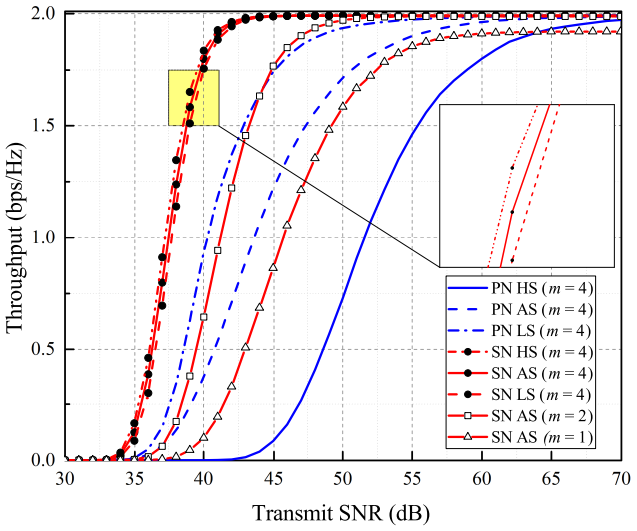

FIGURE 11. Throughput versus the transmit SNR for the PN and SN over different fading parameters.

CP compared to η. Another interesting observation is that the curves corresponding to $\eta = 1$ and $\Phi = 10$ in the PN and SN plots are close to the ideal case of the SNR-independent CSI case, which can be explained by the fact that high η leads to the perfect system performance. Moreover, one can notice that SN has a much higher CP rate than PN which can be explained by the impact of selected system parameters defined in Table 2.

In Fig. 11, we evaluate the impact of various shadowed-Rician and Nakagami-m fading scenarios on the system throughput. Particularly, we assume heavy, average and light shadowed-Rician fading models with parameters (m_i, b_i, Ω_i) set as $(2, 0.063, 0.0005)$, $(5, 0.251, 0.279)$, and $(10, 0.158, 1.29)$, respectively. The figure demonstrates that the light shadowed-Rician fading model allows us to achieve a maximum throughput rate at the relatively lower transmit SNR. Further, it should be noted that the variation of shadowed-Rician parameters does not have a considerable influence on the throughput rate of the secondary users. Therefore, we examine different SUs' throughput rate by varying shape parameter of Nakagami-m fading. Thus, it can be seen that their performance degrades as m decreases.

VI. CONCLUSION

In this article, we have evaluated the performance of NOMA-assisted CSTNs, wherein the SN (limited by ITC) co-shares the available spectrum with the PN. Different from existing works, we have assumed NOMA for both primary and secondary networks and obtained the closed-form CP expressions taking into account the hardware, SIC, and CSI imperfections along with interference noises. Furthermore,

a comparison with the OMA network, which is considered as a benchmark scheme, revealed that the proposed NOMA-based CSTN demonstrates outstanding performance advancement while utilizing the spectrum resource in an efficient manner. The correctness of these derived analytical findings was validated by Monte Carlo simulations. Moreover, the obtained results highlighted the significance of considering HIs at transceivers, especially, when there is a certain tolerance level of the system. The results also demonstrated that the impact of HI on the system performance can be enhanced with the increase of imperfect SIC. Further, we provided closed-form and algorithmic PA solutions in order to guarantee fairness among all users. Finally, the impact of each imperfection on the system performance was examined in terms of the CP and throughput under various system scenarios.

APPENDIX A
SATELLITE PRIMARY NETWORK

In this section, we present the derivation steps for appraising the coverage performance of the NOMA end-users in the PN. The CP can be evaluated using (6) as

$$\begin{aligned}\mathbb{P}_{cov,i}(v) &= \Pr\left[X_i > I(i)\left(\Sigma_i + cY_i\right)\right] \\ &= 1 - \int_0^{\infty} \underbrace{\left(\int_0^{I(i)(\Sigma_i+cY_i)} f_{X_i}(x)\mathrm{d}x\right)}_{A_1} f_Y(y)\mathrm{d}y.\end{aligned} \tag{A.1}$$

where $I(i) = \frac{v}{a_i - b_i v}$. Here, A_1 can be obtained by integrating (2) with the aid of [49, Eq. (3.351.1)] as

$$\begin{aligned}A_1 &= \int_0^{I(i)(\Sigma_i+cY_i)} \sum_{\ell=0}^{m_n-1} \Upsilon x^{\ell} e^{-\partial_n x}\mathrm{d}x = \sum_{\ell=0}^{m_n-1} \Upsilon \frac{\ell!}{\partial_n^{\ell+1}} \\ &- \sum_{\ell=0}^{m_n-1} \Upsilon e^{-I(i)(\Sigma_i+cY_i)\partial_n} \sum_{p=0}^{\ell} \frac{\ell!}{p!} \frac{\left(I(i)\left(\Sigma_i + cY_i\right)\right)^p}{\partial_n^{\ell-p+1}}.\end{aligned} \tag{A.2}$$

Further, let us denote $\Delta = I(i)\left(\Sigma_i + cY_i\right)$, then Δ^p can be expanded using a binomial theorem as $\Delta^p = (I(i))^p \sum_{t=0}^{p} \binom{p}{t} (\Sigma_i)^{p-t} (cY_i)^t$. Now, for the terrestrial interference link, the i.n.i.d. Gamma RVs with shape m_k and scale v parameters are generated using (4). By substituting (A.2) into (A.1) and using Δ^p, the CP can be rewritten as

$$\begin{aligned}\mathbb{P}_{cov,i}(v) &= 1 - \sum_{\ell=0}^{m_n-1} \Upsilon \frac{\ell!}{\partial_n^{\ell+1}} \int_0^{\infty} \frac{y^{m_k-1} e^{-\frac{y}{v}}}{\Gamma(m_k) v^{m_k}} \mathrm{d}y \\ &+ \sum_{\ell=0}^{m_n-1} \sum_{p=0}^{\ell} \frac{\ell!}{p!} \frac{\Upsilon e^{-I(i)\Sigma_i\partial_n}}{\partial_n^{\ell-p+1}} (I(i))^p \sum_{t=0}^{p} \binom{p}{t} \frac{(\Sigma_i)^{p-t}\, c^t}{\Gamma(m_k) v^{m_k}} \\ &\times \int_0^{\infty} (y_i)^{t+m_k-1} e^{-y\left(\frac{1}{v} + I(i)\partial_n c\right)} \mathrm{d}y.\end{aligned} \tag{A.3}$$

Finally, we can express the exact CP with the aid of [49, Eq. (8.310.1)] in its closed form as in (10). ■

APPENDIX B
TERRESTRIAL SECONDARY NETWORK

The term A in (11) can be rewritten as

$$A = 1 - \underbrace{\int_{q=0}^{\infty} f_Q(q) \underbrace{\int_{z=0}^{T_1+T_2Q_j} -f_Z(z)\mathrm{d}z}_{A_1} \mathrm{d}q}_{A_2} \underbrace{\int_{y=0}^{\Lambda} f_Y(y)\mathrm{d}y}_{A_3}. \tag{B.1}$$

The PDFs of Z and Y abide by Nakagami-m statistical model, and Q follows the shadowed-Rician distribution. Therefore, using (4), we obtain $A_1 = 1 - \sum_{p=0}^{m_0-1} \sum_{n=0}^{p} e^{\frac{-T_1-T_2 Q_j}{v_0}} M_A (T_2 Q_j)^n$, where $M_A = e^{\frac{-T_1}{v_0}} \frac{1}{v_0^p \Gamma(p+1)} \binom{p}{n} T_1^{p-n}$. Now, knowing the results of A_1 and using (2), we calculate A_2 with the aid of [49, Eq. (3.351.3)] as

$$\begin{aligned}A_2 &= \left(1 - \sum_{p=0}^{m_0-1} \sum_{n=0}^{p} e^{\frac{-T_1-T_2Q_j}{v_0}} M_A (T_2 Q_j)^n\right) \sum_{\ell=0}^{m_n-1} \Upsilon \int_0^{\infty} q^{\ell} e^{-\partial_n q} \mathrm{d}q \\ &= \sum_{\ell=0}^{m_n-1} \Upsilon \ell! \partial_n^{-\ell-1} - \sum_{\ell=0}^{m_n-1} \sum_{p=0}^{m_0-1} \sum_{n=0}^{p} M_A T_2^n \Upsilon \\ &\times (n+\ell)! \left(\frac{T_2}{v_0} + \partial_n\right)^{-n-\ell-1},\end{aligned} \tag{B.2}$$

and the CDF A_3 can be obtained independently as $\frac{\gamma\left(m_k, \frac{\Lambda}{v}\right)}{\Gamma(m_k)}$. Finally, by inserting A_2 and A_3 into (B.1), we express A in a closed form as in (12).

The term B in (11) can be determined as

$$B = - \int_{q=0}^{\infty} f_Q(q) \underbrace{\int_{y=\Lambda}^{\infty} f_Y(y) \int_0^{J_1 Y + J_2 Y Q_j + J_3} f_Z(z)\mathrm{d}z\mathrm{d}y}_{B_1} \mathrm{d}q. \tag{B.3}$$

Here, using (4) and the CDF of Z, B_1 can be calculated as

$$\begin{aligned}B_1 &= \left(1 - e^{\frac{-J_1 Y - J_2 Y Q_j - J_3}{v_0}} \right. \\ &\left. \times \sum_{p=0}^{m_0-1} \frac{\left(J_3 + Y(J_1 + J_2 Q_j)\right)^p}{v_0^p \Gamma(p+1)}\right) \int_{\Lambda}^{\infty} \frac{y^{m-1} e^{-\frac{y}{v}}}{\Gamma(m) v^m} \mathrm{d}y \\ &= \frac{\Gamma(m, \frac{\Lambda}{v})}{\Gamma(m)} - \sum_{p=0}^{m_0-1} \sum_{t=0}^{p} M_B \left(J_1 + J_2 Q_j\right)^t \\ &\times \int_{\Lambda}^{\infty} \frac{y^t y^{m-1} e^{-y\left(\frac{1}{v} + V_1\right)}}{\Gamma(m) v^m} \mathrm{d}y \\ &= \frac{\Gamma(m, \frac{\Lambda}{v})}{\Gamma(m)} - \sum_{p=0}^{m_0-1} \sum_{t=0}^{p} M_B \\ &\times \underbrace{\left(J_1 + J_2 Q_j\right)^t \frac{\Gamma\left(t+m, \left(\frac{1+vV_1}{v}\right)\Lambda\right)}{\Gamma(m) v^m} \left(\frac{1+vV_1}{v}\right)^{-t-m}}_{B_2},\end{aligned} \tag{B.4}$$

where $M_B = \sum_{p=0}^{m_0-1} \frac{1}{\nu_0^p \Gamma(p+1)} \sum_{t=0}^{p} \binom{p}{t} (J_3)^{p-t}$ and $V_1 = \frac{J_1 + J_2 Q_j}{\nu_0}$.

Now, we need to apply the series representation of the upper incomplete Gamma function given as $\Gamma(b,c) = \Gamma(b)e^{-c}\sum_{i=0}^{b-1}\frac{c^i}{i!}$ [49] and binomial theorem in order to expand B_2 in (B.4). Next, after some algebraic manipulations, we rewrite B_2 as

$$B_2 = \sum_{i=0}^{t} \binom{t}{i} J_1^{t-i} \left(J_2 Q_j\right)^i \sum_{j=0}^{t+m-1} \frac{\Gamma(t+m)\Lambda^j V_2}{\Gamma(m)\nu^m j!} \times e^{-\left(\frac{1}{\nu}+\frac{J_1+J_2Q_j}{\nu_0}\right)\Lambda} \left(1+\Omega Q_j\right)^{j-t-m}, \quad \text{(B.5)}$$

where $V_2 = \left(\frac{\nu_0+\nu J_1}{\nu_0 \nu}\right)^{j-t-m}$ and $\Omega = \frac{\nu J_2}{\nu_0+\nu J_1}$. Thus, B can be rewritten as

$$B = -\frac{\Gamma(m, \frac{\Lambda}{\nu})}{\Gamma(m)} \sum_{\ell=0}^{m_n-1} \Upsilon \int_0^\infty q^\ell e^{-\partial_n q} \mathrm{d}q + \sum_{p=0}^{m_0-1}\sum_{t=0}^{p} M_B \times \sum_{i=0}^{t} \binom{t}{i} J_1^{t-i} J_2^i \frac{\Gamma(t+m)}{\Gamma(m)\nu^m} e^{-\left(\frac{1}{\nu}+\frac{J_1}{\nu_0}\right)\Lambda} \sum_{\ell=0}^{m_n-1}\sum_{j=0}^{t+m-1} \frac{\Lambda^j}{j!} V_2 \Upsilon \times \int_0^\infty \left(1+\Omega Q_j\right)^{-(t+m-j)} q^{i+\ell+1-1} e^{-(\frac{J_2\Lambda}{\nu_0}+\partial_n)q} \mathrm{d}q. \quad \text{(B.6)}$$

Finally, by using the Meijer-G function represented with the aid of [57, Eqs. (7.34.3.46.1) and (7.34.3.271.1)], where $e^{-b\gamma} = G_{0,1}^{1,0}\left(b\gamma|_0^-\right)$ and $(1+c\gamma)^{-d} = \frac{1}{\Gamma(d)} G_{1,1}^{1,1}\left(c\gamma|_0^{1-d}\right)$, and after some algebraic manipulations [49, Eq. (3.351.3)], we obtain the closed-form expression of B as in (13). ■

A. ADDITIONAL INSIGHTS

Considering the complexity of the derived expression for the coverage probability of SUs, it is pertinent to simplify it in order to obtain useful insights about the network performance.

By taking a closer look at (12) and (13), we can note that these two expressions can be greatly simplified if the term C (standing for the interference originating from the satellite) in (8) is eliminated. Considering that $T_2 = \frac{\nu C}{P_s(W_1 - \nu W_2)}$ and $J_2 = \frac{\nu C}{I_{ITC}^{[i]}(W_1-\nu W_2)}$ are directly proportional to C and they will be also eliminated, the coverage probability can be simply expressed as

$$\mathbb{P}_{cov,j}^{\mathrm{SN}}(\nu) = A + B, \quad \text{(B.7)}$$

where

$$A = 1 - \left(1 - e^{-\frac{T_1}{\nu_0}} \sum_{p=0}^{m_0-1} \frac{(T_1)^p}{\nu_0^p \Gamma(p+1)}\right) \frac{\gamma\left(m_k, \frac{\Lambda}{\nu}\right)}{\Gamma(m_k)}, \quad \text{(B.8)}$$

$$B = -\frac{\Gamma(m, \frac{\Lambda}{\nu})}{\Gamma(m)} + e^{\frac{-J_3}{\nu_0}} \sum_{p=0}^{m_0-1} \frac{1}{\nu_0^p \Gamma(p+1)} \sum_{t=0}^{p} \binom{p}{t} J_3^{p-t} J_1^t \times \frac{\Gamma\left(t+m, \left(\frac{1}{\nu}+\frac{J_1}{\nu_0}\right)\Lambda\right)}{\Gamma(m)\nu^m} \left(\frac{1}{\nu}+\frac{J_1}{\nu_0}\right)^{-t-m}. \quad \text{(B.9)}$$

Further, considering the high-SNR approximations for the Λ term in lower and upper incomplete gamma functions as $\gamma_{\mathrm{inc}}(c,d) \approx \frac{d^c}{c}$ and $\Gamma(c,d) \approx \Gamma(c)$, $d \to 0$, we can rewrite A and B as follows

$$A = 1 - \left(1 - e^{-\frac{T_1}{\nu_0}} \sum_{p=0}^{m_0-1} \frac{(T_1)^p}{\nu_0^p \Gamma(p+1)}\right) \frac{\left(\frac{\Lambda}{\nu}\right)^{m_k}}{m_k \Gamma(m_k)}, \quad \text{(B.10)}$$

$$B = e^{\frac{-J_3}{\nu_0}} \sum_{p=0}^{m_0-1} \frac{1}{\nu_0^p \Gamma(p+1)} \sum_{t=0}^{p} \binom{p}{t} J_3^{p-t} \times J_1^t \frac{\Gamma(t+m)}{\Gamma(m)\nu^m} \left(\frac{1}{\nu}+\frac{J_1}{\nu_0}\right)^{-t-m} - 1. \quad \text{(B.11)}$$

Then, we have

$$\mathbb{P}_{cov,j}^{\mathrm{SN}}(\nu) = \sum_{p=0}^{m_0-1} \frac{e^{\frac{-T_1}{\nu_0}} (T_1)^p}{\nu_0^p \Gamma(p+1)} \frac{\left(\frac{\Lambda}{\nu}\right)^{m_k}}{m_k \Gamma(m_k)} - \frac{\left(\frac{\Lambda}{\nu}\right)^{m_k}}{m_k \Gamma(m_k)} + e^{\frac{-J_3}{\nu_0}} \sum_{p=0}^{m_0-1}\sum_{t=0}^{p} \binom{p}{t} \frac{J_3^{p-t} J_1^t}{\nu_0^p \Gamma(p+1)} \times \frac{\Gamma(t+m)}{\Gamma(m)\nu^m} \left(\frac{1}{\nu}+\frac{J_1}{\nu_0}\right)^{-t-m}, \quad \text{(B.12)}$$

where J_3 can be simplified as $J_3 = \frac{\nu\left(1+\bar{\kappa_i}^2\right)\sigma_\epsilon^2}{(\beta_k - \nu\bar{A})}$. Thus, it is clearly seen that increasing the CSI imperfection, *i.e.*, σ_ϵ^2, will lead to the increment of J_3; hence, the exponential term (*i.e.*, $e^{-\frac{J_3}{\nu_0}}$) decreases and consequently leads to the degradation of the system performance, as expected. The HI parameter, $\bar{\kappa_i}$, has a similar but relatively marginal influence.

Furthermore, one can note that Nakagami-m fading severity parameter, m_0, correlates with the summation index p. Particularly, higher m_0 leads to higher p. Then, considering the fact that $J_3 < 1$, its power of p produces an even smaller number, thus, deteriorating the coverage probability. Therefore, it can be concluded that the Nakagami-m fading parameter m_0 leads to the degradation of system performance. Moreover, by noting that P_s is in the denominator of both T_1 and Λ, one can observe that its increment will lead to the deterioration of CP, as expected.

REFERENCES

[1] L. Dai, B. Wang, Z. Ding, Z. Wang, S. Chen, and L. Hanzo, "A survey of non-orthogonal multiple access for 5G," *IEEE Commun. Surveys Tuts.*, vol. 20, no. 3, pp. 2294–2323, 3rd Quart., 2018.
[2] IDC: The Premier Global Market Intelligence Company. *The Growth In Connected IoT Devices*. Accessed: Jun. 18, 2019. [Online]. Available: https://www.idc.com
[3] G. Giambene, S. Kota, and P. Pillai, "Satellite-5G integration: A network perspective," *IEEE Netw.*, vol. 32, no. 5, pp. 25–31, Sep. 2018.
[4] Y. Ruan, R. Zhang, Y. Li, C.-X. Wang, and H. Zhang, "Spectral-energy efficiency tradeoff in cognitive satellite-vehicular networks towards beyond 5G," in *Proc. IEEE Wireless Commun. Netw. Conf. (WCNC)*, Marrakesh, Morocco, Apr. 2019, pp. 1–6.
[5] G. Nauryzbayev, M. Abdallah, and H. Elgala, "On the performance of NOMA-enabled spectrally and energy efficient OFDM (SEE-OFDM) for indoor visible light communications," in *Proc. IEEE 87th Veh. Technol. Conf. (VTC Spring)*, Porto, Portugal, Jun. 2018, pp. 1–5.
[6] G. Nauryzbayev, M. Abdallah, and H. Elgala, "Outage of SEE-OFDM VLC-NOMA networks," *IEEE Photon. Technol. Lett.*, vol. 31, no. 2, pp. 121–124, Jan. 15, 2019.

[7] Y. Akhmetkaziyev, "Coverage analysis of CR-based satellite-terrestrial noma networks with practical system impairments," in *Proc. IEEE Int. Conf. Commun. (ICC),* Montreal, QC, Canada, Jun. 2021, pp. 1–6.

[8] H. Haci, H. Zhu, and J. Wang, "Performance of non-orthogonal multiple access (NOMA) with a novel asynchronous interference cancellation technique," *IEEE Trans. Commun.*, vol. 65, no. 3, pp. 1319–1335, Mar. 2017.

[9] T. Assaf, A. Al-Dweik, M. E. Moursi, and H. Zeineldin, "Exact BER performance analysis for downlink NOMA systems over Nakagami-*M* fading channels," *IEEE Access*, vol. 7, pp. 134539–134555, 2019.

[10] M. Shirvanimoghaddam, M. Dohler, and S. J. Johnson, "Massive non-orthogonal multiple access for cellular IoT: Potentials and limitations," *IEEE Commun. Mag.*, vol. 55, no. 9, pp. 55–61, Sep. 2017.

[11] L. Dai, B. Wang, Y. Yuan, S. Han, I. Chih-lin, and Z. Wang, "Non-orthogonal multiple access for 5G: Solutions, challenges, opportunities, and future research trends," *IEEE Commun. Mag.*, vol. 53, no. 9, pp. 74–81, Sep. 2015.

[12] Y. Saito, Y. Kishiyama, A. Benjebbour, T. Nakamura, A. Li, and K. Higuchi, "Non-orthogonal multiple access (NOMA) for cellular future radio access," in *Proc. IEEE 77th Veh. Technol. Conf. (VTC Spring)*, Dresden, Germany, Jun. 2013, pp. 1–5.

[13] V. Bankey, P. K. Upadhyay, D. B. Da Costa, P. S. Bithas, A. G. Kanatas, and U. S. Dias, "Performance analysis of multi-antenna multiuser hybrid satellite-terrestrial relay systems for mobile services delivery," *IEEE Access*, vol. 6, pp. 24729–24745, 2018.

[14] Y. Ruan, Y. Li, C.-X. Wang, and R. Zhang, "Energy efficient adaptive transmissions in integrated satellite-terrestrial networks with SER constraints," *IEEE Trans. Wireless Commun.*, vol. 17, no. 1, pp. 210–222, Jan. 2018.

[15] K. Guo, K. An, B. Zhang, Y. Huang, D. Guo, G. Zheng, and S. Chatzinotas, "On the performance of the uplink satellite multiterrestrial relay networks with hardware impairments and interference," *IEEE Syst. J.*, vol. 13, no. 3, pp. 2297–2308, Sep. 2019.

[16] Q. Huang, M. Lin, K. An, J. Ouyang, and W. Zhu, "Secrecy performance of hybrid satellite-terrestrial relay networks in the presence of multiple eavesdroppers," *IET Commun.*, vol. 12, no. 1, pp. 26–34, Jan. 2018.

[17] K. Guo, K. An, B. Zhang, Y. Huang, and D. Guo, "Physical layer security for hybrid satellite terrestrial relay networks with joint relay selection and user scheduling," *IEEE Access*, vol. 6, pp. 55815–55827, 2018.

[18] P. K. Sharma, B. Yogesh, and D. Gupta, "Internet of Things-enabled overlay satellite-terrestrial networks in the presence of interference," in *Proc. Nat. Conf. Commun. (NCC)*, Kharagpur, India, Feb. 2020, pp. 1–6.

[19] H. Wei, W. Feng, C. Zhang, Y. Chen, Y. Fang, and N. Ge, "Creating efficient blockchains for the Internet of Things by coordinated satellite-terrestrial networks," *IEEE Wireless Commun.*, vol. 27, no. 3, pp. 104–110, Jun. 2020.

[20] V. A. Siris, Y. Thomas, and G. C. Polyzos, "Supporting the IoT over integrated satellite-terrestrial networks using information-centric networking," in *Proc. 8th IFIP Int. Conf. New Technol., Mobility Secur. (NTMS)*, Larnaca, Cyprus, Nov. 2016, pp. 1–5.

[21] Q. Zhang, K. An, X. Yan, and T. Liang, "Coexistence and performance limits for the cognitive broadband satellite system and mmWave cellular network," *IEEE Access*, vol. 8, pp. 51905–51917, 2020.

[22] X. Yan, K. An, T. Liang, G. Zheng, and Z. Feng, "Effect of imperfect channel estimation on the performance of cognitive satellite terrestrial networks," *IEEE Access*, vol. 7, pp. 126293–126304, 2019.

[23] Y. Ruan, Y. Li, C.-X. Wang, R. Zhang, and H. Zhang, "Energy efficient power allocation for delay constrained cognitive satellite terrestrial networks under interference constraints," *IEEE Trans. Wireless Commun.*, vol. 18, no. 10, pp. 4957–4969, Oct. 2019.

[24] V. Singh, S. Solanki, and P. K. Upadhyay, "Cognitive relaying cooperation in satellite-terrestrial systems with multiuser diversity," *IEEE Access*, vol. 6, pp. 65539–65547, 2018.

[25] P. Lai, H. Bai, Y. Huang, Z. Chen, and T. Liu, "Performance evaluation of underlay cognitive hybrid satellite–terrestrial relay networks with relay selection scheme," *IET Commun.*, vol. 13, no. 16, pp. 2550–2557, Oct. 2019.

[26] J. Xiong, D. Ma, H. Zhao, and F. Gu, "Secure multicast communications in cognitive satellite-terrestrial networks," *IEEE Commun. Lett.*, vol. 23, no. 4, pp. 632–635, Apr. 2019.

[27] Z. Lin, M. Lin, B. Champagne, W.-P. Zhu, and N. Al-Dhahir, "Secure beamforming for cognitive satellite terrestrial networks with unknown eavesdroppers," *IEEE Syst. J.*, early access, Apr. 20, 2020, doi: 10.1109/JSYST.2020.2983309.

[28] Y. Zhou, V. W. S. Wong, and R. Schober, "Coverage and rate analysis of millimeter wave NOMA networks with beam misalignment," *IEEE Trans. Wireless Commun.*, vol. 17, no. 12, pp. 8211–8227, Dec. 2018.

[29] S. Arzykulov, G. Nauryzbayev, T. A. Tsiftsis, and B. Maham, "Performance analysis of underlay cognitive radio nonorthogonal multiple access networks," *IEEE Trans. Veh. Technol.*, vol. 68, no. 9, pp. 9318–9322, Sep. 2019.

[30] S. Arzykulov, G. Nauryzbayev, T. A. Tsiftsis, B. Maham, M. S. Hashmi, and K. M. Rabie, "Underlay spectrum sharing for NOMA relaying networks: Outage analysis," in *Proc. Int. Conf. Comput., Netw. Commun. (ICNC)*, Big Island, HI, USA, Feb. 2020, pp. 897–901.

[31] S. Arzykulov, G. Nauryzbayev, M. S. Hashmi, A. M. Eltawil, K. M. Rabie, and S. Seilov, "Hardware- and interference-limited cognitive IoT relaying NOMA networks with imperfect SIC over generalized non-homogeneous fading channels," *IEEE Access*, vol. 8, pp. 72942–72956, 2020.

[32] X. Yan, H. Xiao, C.-X. Wang, and K. An, "Outage performance of NOMA-based hybrid satellite-terrestrial relay networks," *IEEE Wireless Commun. Lett.*, vol. 7, no. 4, pp. 538–541, Aug. 2018.

[33] S. Xie, B. Zhang, D. Guo, and B. Zhao, "Performance analysis and power allocation for NOMA-based hybrid satellite-terrestrial relay networks with imperfect channel state information," *IEEE Access*, vol. 7, pp. 136279–136289, Sep. 2019.

[34] Z. Lin, M. Lin, J.-B. Wang, T. de Cola, and J. Wang, "Joint beamforming and power allocation for satellite-terrestrial integrated networks with non-orthogonal multiple access," *IEEE J. Sel. Topics Signal Process.*, vol. 13, no. 3, pp. 657–670, Jun. 2019.

[35] N.-L. Nguyen, H.-N. Nguyen, A.-T. Le, D.-T. Do, and M. Voznak, "On performance analysis of NOMA-aided hybrid satellite terrestrial relay with application in small-cell network," *IEEE Access*, vol. 8, pp. 188526–188537, 2020.

[36] M. Jia, Q. Gao, Q. Guo, X. Gu, and X. Shen, "Power multiplexing NOMA and bandwidth compression for satellite-terrestrial networks," *IEEE Trans. Veh. Technol.*, vol. 68, no. 11, pp. 11107–11117, Nov. 2019.

[37] X. Zhang, D. Guo, K. An, Z. Chen, B. Zhao, Y. Ni, and B. Zhang, "Performance analysis of NOMA-based cooperative spectrum sharing in hybrid satellite-terrestrial networks," *IEEE Access*, vol. 7, pp. 172321–172329, 2019.

[38] X. Zhang, B. Zhang, K. An, Z. Chen, S. Xie, H. Wang, L. Wang, and D. Guo, "Outage performance of NOMA-based cognitive hybrid satellite-terrestrial overlay networks by amplify-and-forward protocols," *IEEE Access*, vol. 7, pp. 85372–85381, 2019.

[39] V. Singh, P. K. Upadhyay, and M. Lin, "On the performance of NOMA-assisted overlay multiuser cognitive satellite-terrestrial networks," *IEEE Wireless Commun. Lett.*, vol. 9, no. 5, pp. 638–642, May 2020.

[40] X. Yan, "On the ergodic capacity of NOMA-based cognitive hybrid satellite terrestrial networks," in *Proc. IEEE/CIC Int. Conf. Commun. China (ICCC),* Qingdao, China, Oct. 2017, pp. 1–5.

[41] X. Li, M. Zhao, Y. Liu, L. Li, Z. Ding, and A. Nallanathan, "Secrecy analysis of ambient backscatter NOMA systems under I/Q imbalance," *IEEE Trans. Veh. Technol.*, vol. 69, no. 10, pp. 12286–12290, Oct. 2020.

[42] X. Li, Q. Wang, Y. Liu, T. A. Tsiftsis, Z. Ding, and A. Nallanathan, "UAV-aided multi-way NOMA networks with residual hardware impairments," *IEEE Wireless Commun. Lett.*, vol. 9, no. 9, pp. 1538–1542, Sep. 2020.

[43] B. Selim, S. Muhaidat, P. C. Sofotasios, B. S. Sharif, T. Stouraitis, G. K. Karagiannidis, and N. Al-Dhahir, "Performance analysis of non-orthogonal multiple access under I/Q imbalance," *IEEE Access*, vol. 6, pp. 18453–18468, 2018.

[44] Y. Wu, Y. Gu, and Z. Wang, "Efficient channel estimation for mmWave MIMO with transceiver hardware impairments," *IEEE Trans. Veh. Technol.*, vol. 68, no. 10, pp. 9883–9895, Oct. 2019.

[45] M. Li, B. Selim, S. Muhaidat, P. C. Sofotasios, M. Dianati, P. D. Yoo, J. Liang, and A. Wang, "Effects of residual hardware impairments on secure NOMA-based cooperative systems," *IEEE Access*, vol. 8, pp. 2524–2536, 2020.

[46] H. Wu, Y. Zou, W. Cao, Z. Chen, T. A. Tsiftsis, M. R. Bhatnagar, and R. C. De Lamare, "Impact of hardware impairments on outage performance of hybrid satellite-terrestrial relay systems," *IEEE Access*, vol. 7, pp. 35103–35112, 2019.

[47] V. Singh, S. Solanki, P. K. Upadhyay, D. B. da Costa, and J. M. Moualeu, "Performance analysis of hardware-impaired overlay cognitive satellite–terrestrial networks with adaptive relaying protocol," *IEEE Syst. J.*, early access, Feb. 5, 2020, doi: 10.1109/JSYST.2020.2967836.

[48] X. Tang, K. An, K. Guo, Y. Huang, and S. Wang, "Outage analysis of non-orthogonal multiple access-based integrated satellite-terrestrial relay networks with hardware impairments," *IEEE Access*, vol. 7, pp. 141258–141267, 2019.

[49] I. S. Gradshteyn and I. M. Ryzhik, *Table of Integrals, Series, and Products*, 7th ed. Amsterdam, The Netherlands: Elsevier, 2007.

[50] Y. Gao, B. Xia, Y. Liu, Y. Yao, K. Xiao, and G. Lu, "Analysis of the dynamic ordered decoding for uplink NOMA systems with imperfect CSI," *IEEE Trans. Veh. Technol.*, vol. 67, no. 7, pp. 6647–6651, Jul. 2018.
[51] A. Abdi, "A new simple model for land mobile satellite channels: First- and second-order statistics," *IEEE Trans. Wireless Commun.*, vol. 2, no. 3, pp. 519–528, May 2003.
[52] P. K. Sharma, D. Deepthi, and D. I. Kim, "Outage probability of 3-D mobile UAV relaying for hybrid satellite-terrestrial networks," *IEEE Commun. Lett.*, vol. 24, no. 2, pp. 418–422, Feb. 2020.
[53] K. Guo, K. An, B. Zhang, Y. Huang, and G. Zheng, "Outage analysis of cognitive hybrid satellite-terrestrial networks with hardware impairments and multi-primary users," *IEEE Wireless Commun. Lett.*, vol. 7, no. 5, pp. 816–819, Oct. 2018.
[54] G. Nauryzbayev, M. Abdallah, and K. M. Rabie, "Outage probability of the EH-based full-duplex AF and DF relaying systems in $\alpha-\mu$ environment," in *Proc. IEEE 88th Veh. Technol. Conf. (VTC-Fall)*, Chicago, IL, USA, Aug. 2018, pp. 1–6.
[55] Z. Ding, M. Peng, and H. V. Poor, "Cooperative non-orthogonal multiple access in 5G systems," *IEEE Commun. Lett.*, vol. 19, no. 8, pp. 1462–1465, Aug. 2015.
[56] O. L. Alcaraz Lopez, H. Alves, P. H. Juliano Nardelli, and M. Latva-aho, "Aggregation and resource scheduling in machine-type communication networks: A stochastic geometry approach," *IEEE Trans. Wireless Commun.*, vol. 17, no. 7, pp. 4750–4765, Jul. 2018.
[57] *The Wolfram Functions Site*, Wolfram, London, U.K., Mar. 2020.

YERASSYL AKHMETKAZIYEV is currently pursuing the bachelor's degree in electrical and electronics engineering from Nazarbayev University, Nur-Sultan, Kazakhstan. His research interests include wireless communication systems and satellite-terrestrial networks, with a particular focus on cognitive radio, NOMA, and the IoT. He has served as a reviewer for several conferences in the wireless communications.

GALYMZHAN NAURYZBAYEV (Senior Member, IEEE) received the B.Sc. and M.Sc. (Hons.) degrees in radio engineering, electronics, and telecommunications from the Almaty University of Power Engineering and Telecommunication, Almaty, Kazakhstan, in 2009 and 2011, respectively, and the Ph.D. degree in wireless communications from the University of Manchester, U.K., in 2016. From 2016 to 2018, he held several academic and research positions with Nazarbayev University, Kazakhstan, L.N. Gumilyov Eurasian National University, Kazakhstan, and Hamad Bin Khalifa University, Qatar. In 2019, he joined as an Assistant Professor with Nazarbayev University. His research interests include wireless communication systems, with particular focus on multiuser MIMO systems, cognitive radio, signal processing, energy harvesting, visible light communications, NOMA, and interference mitigation. He served as a technical program committee member for numerous IEEE flagship conferences.

SULTANGALI ARZYKULOV (Member, IEEE) received the B.Sc. degree (Hons.) in radio engineering, electronics and telecommunications from Kazakh National Research Technical University, after K. I. Satpayev, Almaty, Kazakhstan, in June 2010, the M.Sc. degree in communication engineering from The University of Manchester, Manchester, U.K., in 2013, and the Ph.D. degree in science, engineering and technology from Nazarbayev University, Nur-Sultan, Kazakhstan, in 2019. He is currently a Postdoctoral Scholar with the Computer, Electrical and Mathematical Science and Engineering Division, King Abdullah University of Science and Technology, Saudi Arabia. His research interests include wireless communication systems, with a particular focus on cooperative communications, cognitive radio, energy harvesting, interference mitigation, and NOMA.

Dr. Arzykulov acts as a reviewer for several international journals/conferences and served as a technical program committee member for numerous the IEEE communication society flagship conferences.

AHMED M. ELTAWIL (Senior Member, IEEE) received the B.Sc. and M.Sc. degrees (Hons.) from Cairo University, Giza, Egypt, in 1999 and 1997, respectively, and the Ph.D. degree from the University of California at Los Angeles, Los Angeles, in 2003. Since 2005, he has been with the Department of Electrical Engineering and Computer Science, University of California at Irvine, Irvine, where he was a Founder and the Director of the Wireless Systems and Circuits Laboratory. Since 2019, he has also been a Professor with the Computer, Electrical and Mathematical Science and Engineering Division (CEMSE), King Abdullah University of Science and Technology (KAUST), Thuwal, Saudi Arabia. His research interests include low power digital circuit and signal processing architectures with an emphasis on mobile systems.

Dr. Eltawil has been on the technical program committees and steering committees of numerous workshops, symposia, and conferences in the areas of low power computing and wireless communication system design. He received several awards and distinguished grants, including the NSF CAREER grant supporting his research in low power systems.

KHALED M. RABIE (Senior Member, IEEE) received the M.Sc. and Ph.D. degrees in electrical and electronic engineering from The University of Manchester, in 2011 and 2015, respectively. He is currently an Assistant Professor with the Department of Engineering, Manchester Metropolitan University (MMU), U.K. He has worked as a part of several largescale industrial projects and has published more than 100 journal and conference articles (mostly IEEE). His current research interest includes next-generation wireless communication systems. He serves regularly on the technical program committee (TPC) for several major IEEE conferences, such as GLOBECOM, ICC, and VTC. He is also a Fellow of the U.K. Higher Education Academy (FHEA). He has received numerous awards over the past few years in recognition of his research contributions including the Best Student Paper Award at the IEEE ISPLC, TX, USA, 2015, the MMU Outstanding Knowledge Exchange Project award of 2016, and IEEE Access Editor of the month award for August 2019. He serves as an Editor for the IEEE Communications Letters, an Associate Editor for IEEE Access, an Area Editor for *Physical Communications* (Elsevier), and an Executive Editor for the Transactions on Emerging Telecommunications Technologies.

XINGWANG LI (Senior Member, IEEE) received the B.Sc. degree from Henan Polytechnic University, Jiaozuo, China, in 2007, the M.Sc. degree from the University of Electronic Science and Technology of China, in 2010, and the Ph.D. degree from the Beijing University of Posts and Telecommunications, in 2015. From 2010 to 2012, he was an Engineer with Comba Telecom Ltd., Guangzhou, China. From 2017 to 2018, he was a Visiting Scholar with Queen's University Belfast, Belfast, U.K. He is currently an Associate Professor with the School of Physics and Electronic Information Engineering, Henan Polytechnic University. His research interests include MIMO communication, cooperative communication, hardware constrained communication, non-orthogonal multiple access, physical layer security, unmanned aerial vehicles, and the Internet-of-Things. He has served as many TPC/co-chair such as IEEE GLOBECOM, IEEE/CIC ICCC, IEEE WCNC, IEEE VTC, and IEEE/IET CSNDSP. He is currently an Editor on the Editorial Board of IEEE Access, *Computer Communications*, *Physical Communication*, *IET Quantum Communication*, and *KSII Transactions on Internet and Information Systems*. He is also a Lead Guest Editor of the special issue on "Recent Advances in Physical Layer Technologies for 5G-Enabled Internet of Things" of *Wireless Communications and Mobile Computing*.